

pubs.acs.org/macroletters Letter

Porous Fibers Templated by Melt Blowing Cocontinuous Immiscible Polymer Blends

Aditya Banerji, Kailong Jin, Mahesh K. Mahanthappa, Frank S. Bates,* and Christopher J. Ellison*



Cite This: ACS Macro Lett. 2021, 10, 1196–1203



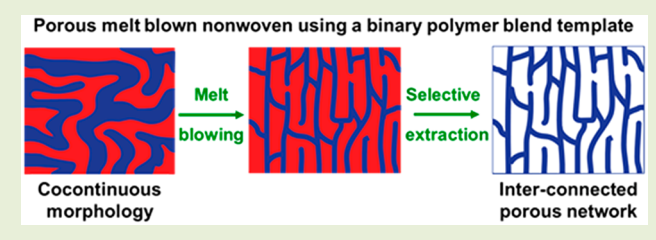
ACCESS

Metrics & More



Supporting Information

ABSTRACT: We report a scalable melt blowing method for producing porous nonwoven fibers from model cocontinuous polystyrene/high-density polyethylene polymer blends. While conventional melt compounding of cocontinuous blends typically produces domain sizes $\sim 1-10~\mu\text{m}$, melt blowing these blends into fibers reduces those dimensions up to 35-fold and generates an interpenetrating domain structure. Inclusion of $\leq 1~\text{wt}$ % of a block copolymer compatibilizer in these blends crucially enables access to



smaller domain sizes in the fibers by minimizing thermodynamically-driven blend coarsening inherent to cocontinuous blends. Selective solvent extraction of the sacrificial polymer phase yielded a network of porous channels within the fibers. Fiber surfaces also exhibited pores that percolate into the fiber interior, signifying the continuous and interconnected nature of the final structure. Pore sizes as small as ~ 100 nm were obtained, suggesting potential applications of these porous nonwovens that rely on their high surface areas, including various filtration modules.

Tonwoven fiber mats exhibit randomly dispersed fibers held together by physical entanglements and/or surface contact forces without any knitting or weaving. 1,2 Nonwoven products constitute a \$50 billion industry with wide-ranging applications such as disposable medical and safety products, tissue engineering scaffolds, and filtration media, among others.^{2,3} Melt blowing is a high-throughput and economical approach widely used in the production of synthetic nonwovens from polymer melts in a single step. Accordingly, this process accounts for more than 10% of global nonwovens production. 4-8 During melt blowing, a polymer melt is extruded through die orifices and drawn into molten polymer filaments using heated high-velocity air jets. During flight, the entrained ambient air rapidly cools the molten filaments below their solidification temperature, either a glass transition temperature (T_g) or crystallization temperature $(T_c)^{4-10}$ to generate solid fibers that deposit on a collector. Typically, linear semicrystalline thermoplastic polymers, such as polyethylene, polypropylene, and polyesters, are used by virtue of their low cost, suitable melt processability, and good thermal and chemical resistance. 1,4-

Melt blown nonwovens with average fiber diameters ranging from $\sim 2-30~\mu m$ are widely employed in applications where a high specific surface area (*i.e.*, surface-to-volume ratio) and interconnected pores between fibers are of critical importance. For example, air filtration modules require high surface area and significant interconnected pore space to effectively capture particulates with a low pressure drop. Fiber-based lithiumion battery separators also benefit from higher surface areas and interconnected pore structures, which facilitate greater electrolyte penetration for improved power performance.

Since the specific surface area of a fiber scales inversely with diameter, significant research efforts have been dedicated to reducing fiber diameters, usually with the goal of producing nanofibers. For instance, a reduction in average fiber diameter from 5 μ m to 500 nm results in 10-fold increase in the specific surface area. Most of these efforts for producing nanofibers focus on electrospinning and centrifugal spinning, with significantly less emphasis on melt blowing. ²²

An alternative approach to enhancing fiber mat specific surface area is to incorporate a pore structure into the fibers. Previously reported approaches to produce porous fibers have exclusively relied on electrospinning and centrifugal spinning. 23–29 For example, Doan et al. and Lu et al. spun fibers from a polymer solution comprising a volatile solvent (e.g., polystyrene dissolved in dimethylformamide or tetrahydrofuran) under conditions that induced rapid solvent evaporation to achieve porous fibers. The pore formation was attributed to a combination of vapor-induced phase separation (VIPS) and formation of breath figures by water vapor condensation due to evaporative cooling during fiber spinning. 28,29 Another approach by Grena et al. involves thermally-induced phase separation (TIPS) of a polyvinylidene fluoride dissolved in propylene carbonate at 150 °C upon cooling below the upper

Received: July 12, 2021 Published: September 20, 2021





critical solution temperature during thermal drawing from a heated reservoir.³⁰ These strategies are limited by their dependence on dilute polymer solutions in organic solvents that leads to low process-throughput as well as volatile organic compound (VOC) emissions arising from significant solvent evaporation during fiber spinning. Thus, it is highly desirable to develop a melt-based approach for producing fibers with internal porous networks.

In this study, we introduce a new approach to produce melt blown nonwovens with interconnected, percolating porous network morphologies within the fibers. This approach leverages cocontinuous morphologies obtained by melt blending two immiscible polymers as a template for the porous structure. Cocontinuous morphologies, in which both polymers form interpenetrating continuous phases, form in immiscible binary polymer blends over small compositional windows around the phase inversion point. 31-34 On either side of the phase inversion point, droplet-in-matrix morphologies are observed where the isolated minority phase droplets are dispersed in a continuous majority phase. The phase inversion point and width of the cocontinuous composition window depend on several factors, such as the melt viscosity, viscosity ratio and interfacial tension. ^{33–36} By considering these factors, suitable compositions for generating a cocontinuous morphology by melt blending have been identified for many model binary polymer blends. As illustrated in Figure 1, melt blowing transforms the cocontinuous morphology in the polymer blend feed into slightly oriented and smaller percolating domains

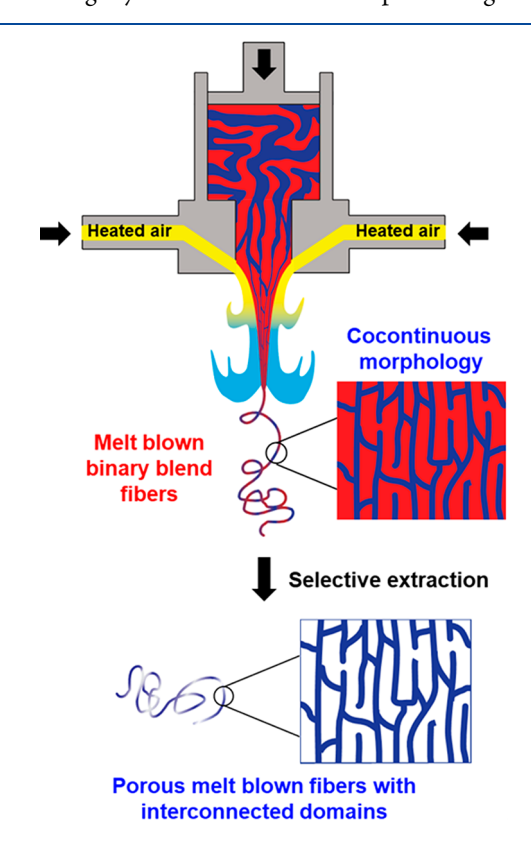


Figure 1. Porous fiber fabrication by melt blowing an immiscible binary polymer blend, in which the cocontinuous morphology of the blend feed is transformed into smaller, slightly oriented, and interconnected domains within the resulting fibers. Selective extraction of the sacrificial polymer (red) then yields a network of porous channels across the entire fiber cross-section.

within the fibers. Subsequent selective extraction of a sacrificial polymer component by solvent washing thus generates porous fibers.

Polymer blends of polystyrene (PS) and high-density polyethylene (HDPE) were chosen as a model system, where PS is the sacrificial component. Details of the materials and experimental procedures are provided in the Supporting Information and Figure S2. Multiple blend compositions ranging from 35/65 to 65/35 wt % PS/HDPE were first studied to identify the cocontinuity window. Accordingly, the cocontinuous morphology obtained after melt blending 60/40 wt % PS/HDPE at 250 °C was chosen for all subsequent studies reported here. The formation of a cocontinuous morphology was corroborated by SEM imaging of cryofractured specimens that were subjected to selective extraction of PS with tetrahydrofuran (THF) solvent at 50 °C (Figure 2a).

60/40 wt % PS/HDPE

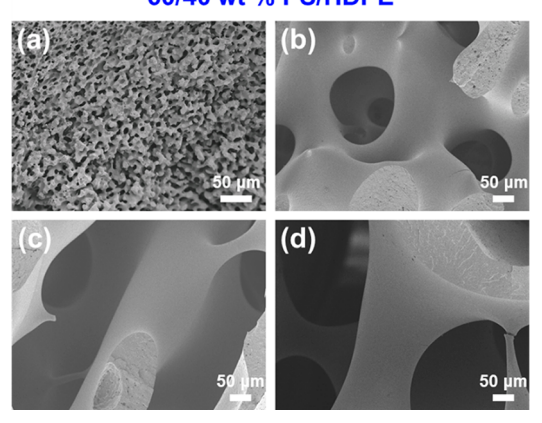


Figure 2. Representative SEM images of the cocontinuous morphology obtained by melt blending 60/40 wt % PS/HDPE at 250 °C for 15 min and annealing at 250 °C for (a) 0 min (asblended), (b) 5, (c) 10, and (d) 15 min.

The cocontinuous nature was further confirmed by removal of $\sim \! 100\%$ of the PS mass from the blend pellets by solvent extraction without disintegrating the self-supporting HDPE phase.

However, the PS/HDPE cocontinuous morphology is inherently unstable and undergoes blend coarsening on static melt annealing.^{37–40} The mobility of the polymer melt enables the interfacial tension-driven retraction and coalescence of the cocontinuous domains that concomitantly reduces the interfacial area and progressively increases the domain size during static annealing. 41-44 In some instances, the cocontinuous morphology ultimately breaks up into a droplet-in-matrix morphology, similar to the classical breakup of a Newtonian fluid thread due to a surface tension-driven Rayleigh instability. 43,44 In our experimental apparatus, some degree of unavoidable coarsening occurs because the polymer blend resides for ~10 min as a near static melt at elevated temperatures prior to reaching the melt blowing die. Static annealing experiments were thus performed at 250 °C to mimic the melt blowing conditions in this study, revealing the progression of blend coarsening. Figure 2b-d shows that the PS/HDPE blend domain sizes increased by a factor of ~25 after a static annealing time of 15 min. Such domain enlargement is undesirable because larger domains in the polymer melt feed will limit the smallest achievable pore sizes

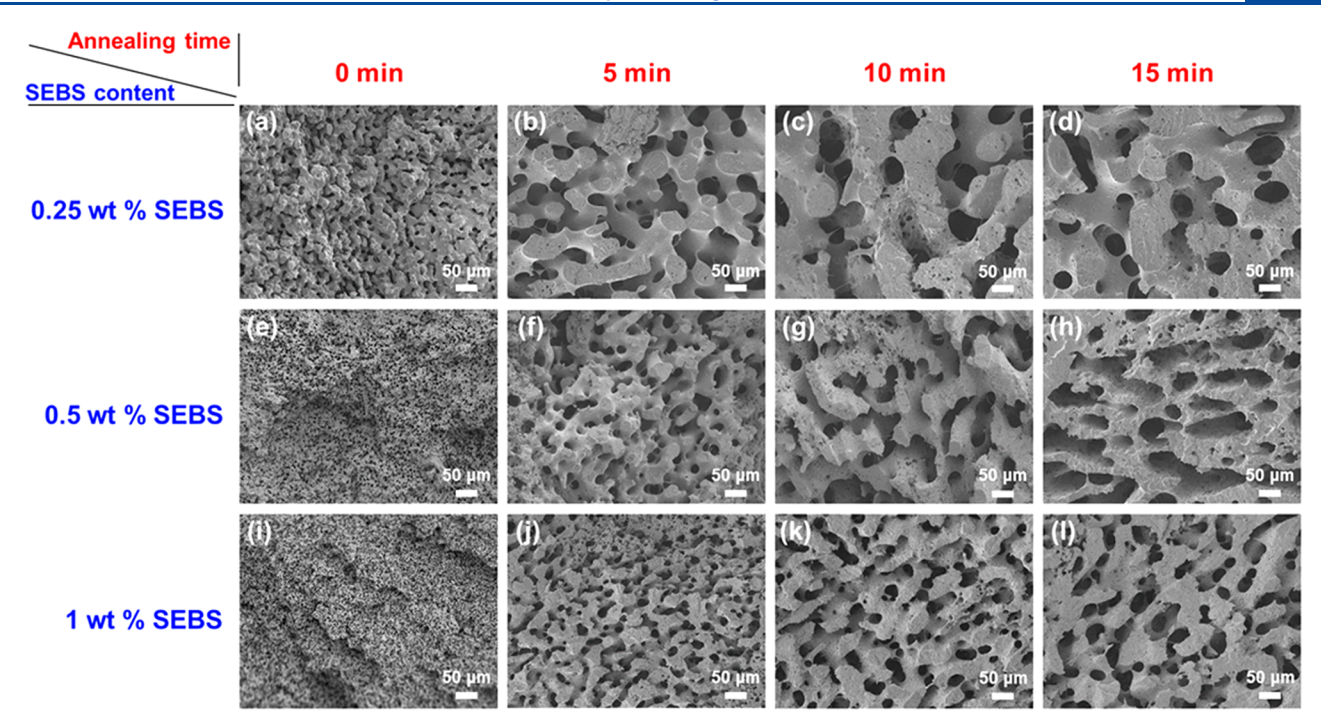


Figure 3. Representative SEM images of the time-dependent cocontinuous morphologies developed during static annealing obtained by melt blending 60/40 wt % PS/HDPE at 250 °C for 15 min, followed by cryofracturing and PS extraction with THF, containing (a–d) 0.25 wt % SEBS, (e–h) 0.5 wt % SEBS, and (i–l) 1 wt % SEBS. In each case, the images presented from left to right represent blends annealed at 250 °C for 0 min (as-blended), 5, 10, and 15 min, respectively.

in the fibers after melt blowing, which dictate their potential applications. 45,46

Generally, blend domain sizes can be reduced by addition of high molecular weight compatibilizer agents, such as block copolymers, that localize at interfaces between polymer phases reducing interfacial tension and promoting domain breakup during blend formation. Furthermore, blend domain coarsening during subsequent annealing (e.g., in the melt blowing feed) is expected to be suppressed by the addition of a block copolymer compatibilizer through steric stabilization. Theoretical treatments indicate that the domain coarsening rate, Γ , can be defined as, 39,43

$$\Gamma = \beta \frac{\gamma}{\eta_{\text{blend}}} \tag{1}$$

where γ is the interfacial tension between two polymers, $\eta_{\rm blend}$ is the blend zero-shear viscosity and β is a dimensionless factor. Equation 1 indicates that reducing the interfacial tension by inclusion of a compatibilizer will lower the coarsening rate. In summary, the combination of these two effects (*i.e.*, smaller domains after initial blend formation and suppressed domain coarsening) is expected to template smaller internal pore sizes in the melt blown fiber.

A triblock copolymer of polystyrene-block-poly(ethylene-ran-butylene)-block-polystyrene (SEBS) was chosen as a compatibilizer, where the polyolefin midblock is miscible with HDPE. Figure 3 shows the time-dependent morphology evolution of cocontinuous PS/HDPE blends with different SEBS contents after static annealing at 250 °C. These results indicate that addition of as little as 0.25 wt % SEBS, significantly minimizes blend coarsening. The results presented in Figure 2 and Figure 3 are quantitatively summarized in Figure 4 by measuring the characteristic domain size, ξ (t), for

the different blend compositions. ξ for a cocontinuous domain can be defined as, $^{50-52}$

$$\xi = \frac{A}{L_{\text{int}}} \tag{2}$$

where A is the total area, and $L_{\rm int}$ is the total interfacial length determined by SEM image analysis (see Supporting Information and Figure S1 for analysis details). Figure 4a demonstrates that the characteristic domain size ξ (t = 0 min) of the "as-blended" PS/HDPE after melt blending decreased from 9.2 µm with no SEBS to 2.5 µm for 1 wt % SEBS. This observation directly reflects the role of lower melt interfacial tension that enables more efficient domain size reduction during melt blending. Furthermore, Figure 4b shows that the addition of SEBS significantly suppresses domain coarsening during static sample annealing. Γ values for different blend compositions were obtained from the slopes of the linear fits of ξ (t), as shown in Figure 4b. Γ decreased from 16.8 μ m/min for PS/HDPE to 1.6, 1.4, and 1.1 μ m/min for blends with 0.25, 0.5, and 1 wt % SEBS, respectively. As a result, cocontinuous domains with much smaller ξ values were obtained even after 10−15 min of annealing at 250 °C. Figure 4 also indicates that ξ can be easily modified based on the SEBS content in the binary blends. For example, ξ (t = 10min) decreased from 176 μ m with no SEBS to 31 μ m with 0.25 wt % SEBS, with a further 2-fold domain size reduction at 1 wt % SEBS loading in the PS/HDPE blends. The ability to tune the domain sizes in the polymer feed is of considerable importance because it potentially translates into a similar tunability of the internal pore sizes in the resulting melt blown fibers.

Melt blowing experiments were performed to understand how the cocontinuous domains of the various binary blends transform upon drawing in the melt state in the absence and

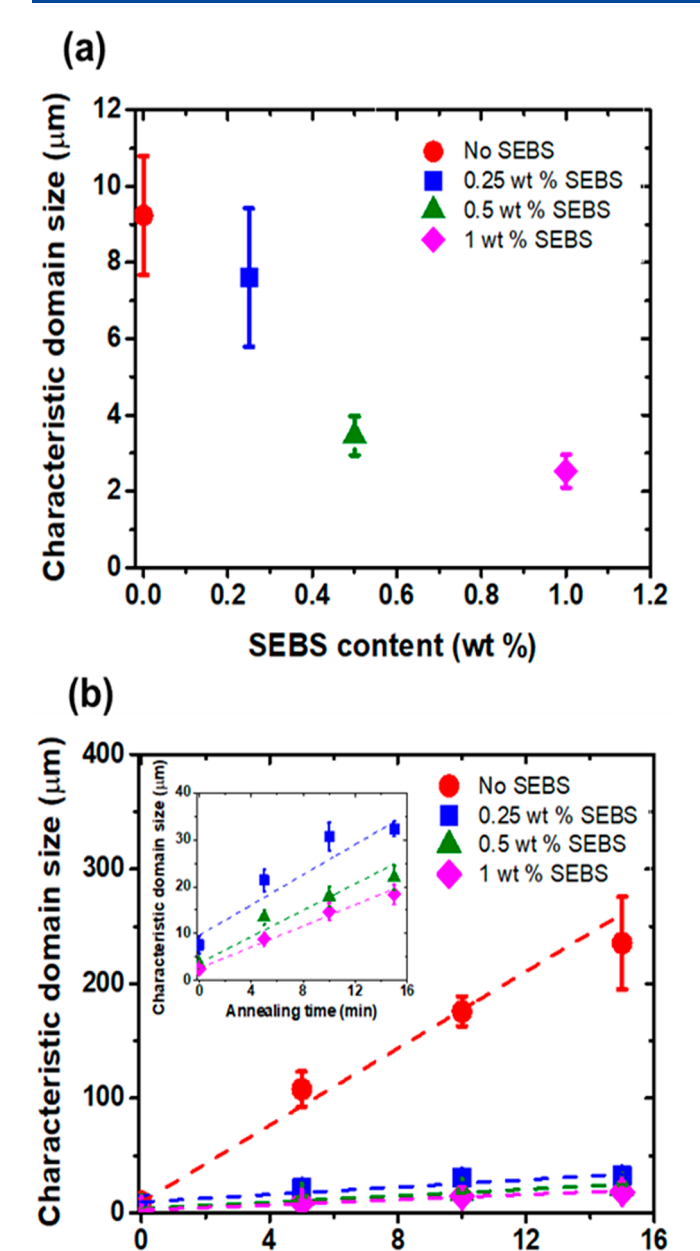


Figure 4. Variation of the characteristic domain size, ξ (t), of different PS/HDPE/SEBS blends as a function of (a) SEBS content (obtained after melt blending) and (b) annealing time at 250 °C. The dashed lines represent the best fit line through all data points. Error bars are standard deviations from at least three independent measurements.

Annealing time (min)

presence of the block copolymer additive. Three blend compositions: 60/40 wt % PS/HDPE, 60/40/0.25 wt % PS/HDPE/SEBS, and 60/40/1 wt % PS/HDPE/SEBS were melt blown using a lab-scale apparatus equipped with a single-hole die having a $400~\mu m$ orifice. 9,17 The melt blowing temperatures ($T_{\rm mb}$) of the different blends were selected such that $\eta_{\rm blend}$ = $150-200~{\rm Pa}\cdot{\rm s}$, a range considered necessary for melt blowing (Figure S3). 5,8 Accordingly, $T_{\rm mb}$ values were determined to be 250, 260, and 280 °C for PS/HDPE, PS/HDPE/0.25 wt % SEBS, and PS/HDPE/1 wt % SEBS blends, respectively (Figure S3). Additional details of the melt blowing apparatus and experimental conditions are provided in the Supporting Information. The porous nonwoven mats after PS extraction

obtained from the three blends display uniform fiber morphologies without any fiber fusion or surface undulations (Figures 5a-c). Statistical analyses of the fiber diameters, which are based on fitting a log-normal distribution function to at least 100 fiber diameter measurements for each sample (see Supporting Information for details), are provided in Figure SS. Additionally, the fiber surfaces exhibited open channels formed on THF extraction of the PS domains (Figure S4). Notably, the porous fiber mats were sufficiently flexible to be easily wrapped around a glass scintillation vial and did not appear to be brittle during handling.

To study the internal fiber morphology, SEM images of fiber cross sections were obtained by cryofracturing the fibers embedded in an epoxy matrix followed by selective extraction of PS by soaking in THF at 50 °C for 30 min. Figure 5d-i shows the formation of porous channels across the entire fiber cross-section after PS extraction at all the blend compositions. To ensure appropriate comparison of the average pore sizes, SEM image analyses were performed on fibers of similar diameters (\sim 32 μ m). As expected, fibers obtained from PS/ HDPE blends (Figure 5d, g) exhibited the largest average pore size of 1.1 μ m because of the significant amount of coarsening prior to reaching the melt blowing die. In contrast, considerably smaller average pore dimensions were observed in fibers obtained from the SEBS-containing PS/HDPE blends (Figure 5e, f and 5h, i) with sizes of 189 and 136 nm in the presence of 0.25 and 1 wt % SEBS, respectively. The reduction in the average pore size with increasing SEBS content validates our hypothesis that the pore sizes can be tuned by suitably varying the compatibilizer content in the polymer blend feed. Figure 5 also shows that for all blend compositions, larger pores are found near the center of the fiber cross-section with relatively smaller pores near the periphery. This distribution of pore sizes may arise due to the radial shear stress gradient generated in the polymer melt extrudate during fiber drawing. As compared to the center of the fiber, the expected higher shear rates near the fiber surface drive enhanced domain elongation to produce smaller pore sizes. In contrast, lower shear rates at the center of the fiber produces a less domain elongation, yielding larger pores. Notably, these pore sizes are situated within the characteristic pore size ranges of both microfiltration (100 nm to 10 μ m) and (5-500 nm) ultrafiltration systems. 45,46 Figure 5g also shows evidence of nanofibers dispersed within the larger pores of PS/HDPE fibers. This observation indicates that a small fraction of the HDPE phase in the neat blend feed transforms into droplets dispersed in the PS matrix during coarsening, possibly due to domains that did not incorporate into the cocontinuous structure and/or surface tension-driven Rayleigh instabilities of some fraction of highly elongated structures. Subsequent drawing of these droplets during melt blowing yields nanofibers, in a manner similar to that reported by Zuo et al. and Wang et al. ^{17,53} In contrast, dispersed nanofibers were not present in the melt blown fibers obtained from compatibilized blends. This observation reiterates the deleterious effect of coarsening and highlights the importance of stabilizing the cocontinuous morphology template to produce porous melt blown fibers.

Figure 6a, c shows the internal axial sections of the melt blown fibers after PS extraction obtained from two PS/HDPE blends containing 0.25 and 1 wt % SEBS. Both cases exhibited \sim 150–300 nm wide pores along the fiber axis, suggesting that the internal channels are interconnected throughout the length

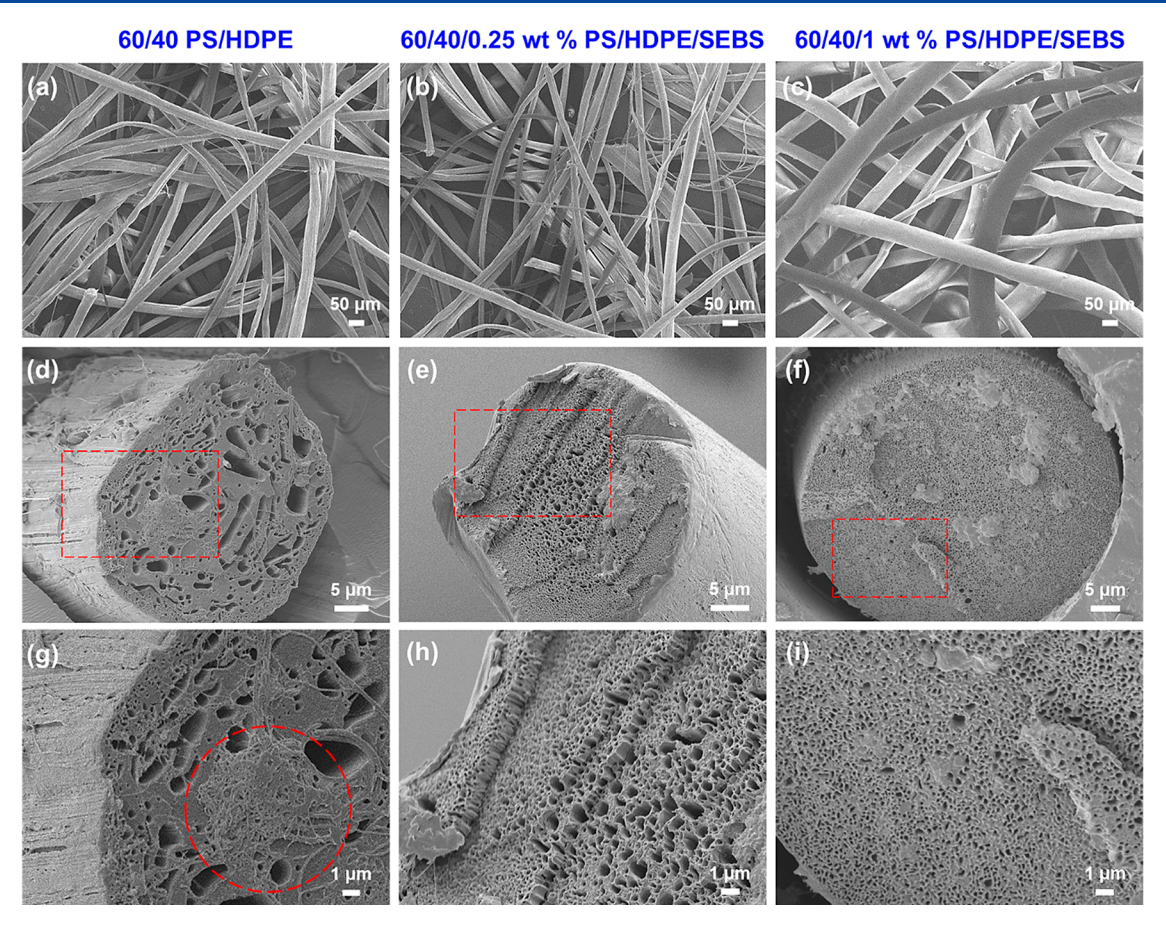


Figure 5. Representative SEM images of (a-c) porous melt blown fibers and (d-i) associated cross sections of cryofractured fibers obtained from (left) 60/40 wt % PS/HDPE, (middle) 60/40/0.25 wt % PS/HDPE/SEBS, and (right) 60/40/1 wt % PS/HDPE/SEBS blends. SEM images in panels g-i are magnified views of the areas marked by red dotted rectangles in panels d-f. The area marked by the red circle in panel g shows evidence of internal nanofibers. All the fiber specimens were imaged after selective extraction of PS.

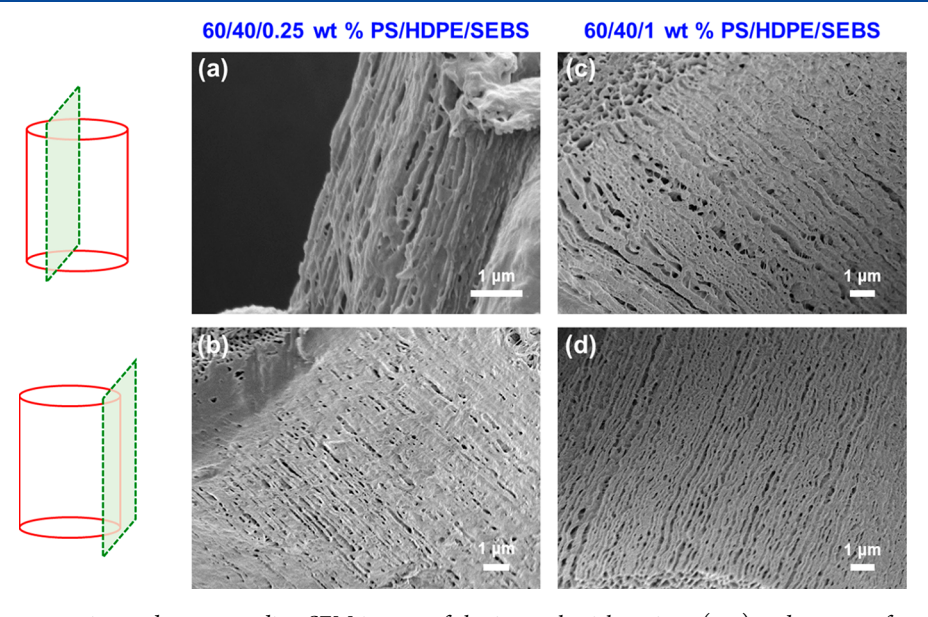


Figure 6. Schematic representation and corresponding SEM images of the internal axial sections (top) and outer surfaces (bottom) of the melt blown fibers obtained from (a, b) 60/40/0.25 wt % PS/HDPE/SEBS and (c, d) 60/40/1 wt % PS/HDPE/SEBS blends.

of the fiber. Figure 6b, d also reveals the existence of porous channels \sim 200 nm in size at the fiber surfaces that appear to percolate into the fiber interior. These two observations strongly suggest the continuous nature of the porous domains

within the fibers, which was corroborated by $\sim 100\%$ PS mass extraction on soaking the fibers in THF without disintegrating the resulting porous HDPE fibers. Such quantitative extraction of the PS component would not be possible if the PS domains

were not continuous throughout the fibers. Differential scanning calorimetry (DSC) and proton nuclear magnetic resonance (¹H NMR) spectrometry analysis (see Supporting Information, Figures S6 and S7) also validated the complete removal of PS from the fiber mat after solvent extraction. The T_{σ} of PS at ~105 °C and ¹H NMR peaks corresponding to the PŠ aromatic rings (6.4–7.4 ppm) are both absent after soaking the fiber mats in THF. An enticing aspect of the porous nonwovens reported here is the formation of hierarchical pore structures, by virtue of combining larger micrometer-sized pores from the inter-fiber spacing in the mat with smaller nanometer-sized pores available due to the porous nature of individual fibers. Such nonwoven mats with hierarchical pores could be a potential alternative to the asymmetric configuration commonly used in nonwoven-based products, which is obtained by stacking multiple nonwoven mats of different fiber diameters and porosities.^{2,34,55}

In summary, we have demonstrated an approach to produce porous nonwoven fibers by melt blowing a cocontinuous binary polymer blend. To the best of our knowledge, this is the first report of porous nonwoven fibers produced by any polymer melt-based fiber processing technique. The cocontinuous morphology obtained by melt blending two immiscible polymers was used as a template to generate interconnected domains after melt blowing. The domain size and extent of coarsening could be controlled by the addition of small amounts of a block copolymer compatibilizer. Selective extraction of the sacrificial polymer component yielded interconnected porous channels across the entire fiber crosssection with pore sizes as small as ~100 nm, suggesting the ability to produce porous nonwovens with hierarchical pore structures within and between fibers. While we chose the PS/ HDPE model blend out of convenience, one can envision that porous fibers could also be obtained using a binary blend comprising a water-soluble polymer where the pore structures can be revealed by washing with water instead of organic solvents.^{21,53} Significant research opportunities exist to fully understand and exploit the potentially unique capabilities of these nonwovens for numerous applications. For example, we anticipate that the hierarchical porosity of the fiber mats may offer improved performance as active layers in biofiltration, air filtration, and fuel/oil filtration modules.

ASSOCIATED CONTENT

3 Supporting Information

The Supporting Information is available free of charge at https://pubs.acs.org/doi/10.1021/acsmacrolett.1c00456.

Experimental and characterization details as well as additional analytical analyses (PDF)

AUTHOR INFORMATION

Corresponding Authors

Frank S. Bates — Department of Chemical Engineering and Materials Science, University of Minnesota, Minneapolis, Minnesota 55455, United States; oocid.org/0000-0003-3977-1278; Email: bates001@umn.edu

Christopher J. Ellison – Department of Chemical Engineering and Materials Science, University of Minnesota, Minneapolis, Minnesota 55455, United States; oorcid.org/0000-0002-0393-2941; Email: cellison@umn.edu

Authors

Aditya Banerji — Department of Chemical Engineering and Materials Science, University of Minnesota, Minneapolis, Minnesota 55455, United States; orcid.org/0000-0003-0654-9195

Kailong Jin — Department of Chemical Engineering and Materials Science, University of Minnesota, Minneapolis, Minnesota 55455, United States; Department of Chemical Engineering, Arizona State University, Tempe, Arizona 85287, United States; orcid.org/0000-0001-5428-3227

Mahesh K. Mahanthappa – Department of Chemical Engineering and Materials Science, University of Minnesota, Minneapolis, Minnesota 55455, United States; orcid.org/ 0000-0002-9871-804X

Complete contact information is available at: https://pubs.acs.org/10.1021/acsmacrolett.1c00456

Notes

The authors declare no competing financial interest.

ACKNOWLEDGMENTS

We gratefully acknowledge Cummins Filtration for financial support. Part of this work (SEM) was carried out in the Characterization Facility, University of Minnesota, which receives partial support from the NSF through the MRSEC (Award DMR-2011401) and the NNCI (Award ECCS-2025124) programs. We thank Xiayu Peng for her assistance with the high-temperature NMR studies.

REFERENCES

- (1) Zhang, D. Advances in Filament Yarn Spinning of Textiles and Polymers; Woodhead Publishing Ltd: Cambridge, UK, 2014.
- (2) Russell, S. Handbook of nonwovens; Woodhead Publishing Ltd: Cambridge, UK, 2007.
- (3) Albrecht, W.; Fuchs, H.; Kittelmann, W. Nonwoven Fabrics: Raw Materials, Manufacture, Applications, Characteristics, Testing Processes; John Wiley & Sons: New York, 2006.
- (4) Wente, V. A. Superfine Thermoplastic Fibers. *Ind. Eng. Chem.* **1956**, 48, 1342–1346.
- (5) Ellison, C. J.; Phatak, A.; Giles, D. W.; Macosko, C. W.; Bates, F. S. Melt blown nanofibers: Fiber diameter distributions and onset of fiber breakup. *Polymer* **2007**, *48*, 3306–3316.
- (6) Nayak, R.; Kyratzis, I. L.; Truong, Y. B.; Padhye, R.; Arnold, L. Structural and mechanical properties of polypropylene nanofibres fabricated by meltblowing. *J. Text. Inst.* **2015**, *106*, 629–640.
- (7) Yesil, Y.; Bhat, G. S. Structure and mechanical properties of polyethylene melt blown nonwovens. *Int. J. Cloth. Sci. Technol.* **2016**, 28, 780–793.
- (8) Tan, D. H.; Zhou, C.; Ellison, C. J.; Kumar, S.; Macosko, C. W.; Bates, F. S. Meltblown fibers: Influence of viscosity and elasticity on diameter distribution. *J. Non-Newtonian Fluid Mech.* **2010**, *165*, 892–
- (9) Jin, K.; Kim, S.-s.; Xu, J.; Bates, F. S.; Ellison, C. J. Melt-Blown Cross-Linked Fibers from Thermally Reversible Diels—Alder Polymer Networks. *ACS Macro Lett.* **2018**, *7*, 1339—1345.
- (10) Jin, K.; Banerji, A.; Kitto, D.; Bates, F. S.; Ellison, C. J. Mechanically Robust and Recyclable Cross-linked Fibers from Melt Blown Anthracene-Functionalized Commodity Polymers. *ACS Appl. Mater. Interfaces* **2019**, *11*, 12863–12870.
- (11) Yesil, Y.; Bhat, G. S. Porosity and barrier properties of polyethylene meltblown nonwovens. *J. Text. Inst.* **2017**, *108*, 1035–1040
- (12) Hassan, M. A.; Yeom, B. Y.; Wilkie, A.; Pourdeyhimi, B.; Khan, S. A. Fabrication of nanofiber meltblown membranes and their filtration properties. *J. Membr. Sci.* **2013**, *427*, 336–344.

- (13) Gibson, P.; Schreuder-Gibson, H.; Rivin, D. Transport properties of porous membranes based on electrospun nanofibers. *Colloids Surf., A* **2001**, *187*–*188*, 469–481.
- (14) Wang, H.; Zhang, Y.; Gao, H. P.; Jin, X. Y.; Xie, X. H. Composite melt-blown nonwoven fabrics with large pore size as Liion battery separator. *Int. J. Hydrogen Energy* **2016**, *41*, 324–330.
- (15) Choi, S. W.; Jo, S. M.; Lee, W. S.; Kim, Y.-R. An Electrospun Poly(vinylidene fluoride) Nanofibrous Membrane and Its Battery Applications. *Adv. Mater.* **2003**, *15*, 2027–2032.
- (16) Drabek, J.; Zatloukal, M. Meltblown technology for production of polymeric microfibers/nanofibers: A review. *Phys. Fluids* **2019**, *31*, 091301.
- (17) Zuo, F.; Tan, D. H.; Wang, Z.; Jeung, S.; Macosko, C. W.; Bates, F. S. Nanofibers from Melt Blown Fiber-in-Fiber Polymer Blends. *ACS Macro Lett.* **2013**, *2*, 301–305.
- (18) Xue, J.; Wu, T.; Dai, Y.; Xia, Y. Electrospinning and Electrospun Nanofibers: Methods, Materials, and Applications. *Chem. Rev.* **2019**, *119*, 5298–5415.
- (19) Huang, Z.-M.; Zhang, Y. Z.; Kotaki, M.; Ramakrishna, S. A review on polymer nanofibers by electrospinning and their applications in nanocomposites. *Compos. Sci. Technol.* **2003**, *63*, 2223–2253.
- (20) Ramakrishna, S.; Fujihara, K.; Teo, W.-E.; Yong, T.; Ma, Z.; Ramaseshan, R. Electrospun nanofibers: solving global issues. *Mater. Today* **2006**, *9*, 40–50.
- (21) Jin, K.; Eyer, S.; Dean, W.; Kitto, D.; Bates, F. S.; Ellison, C. J. Bimodal Nanofiber and Microfiber Nonwovens by Melt-Blowing Immiscible Ternary Polymer Blends. *Ind. Eng. Chem. Res.* **2020**, *59*, 5238–5246.
- (22) Kenry; Lim, C. T. Nanofiber technology: current status and emerging developments. *Prog. Polym. Sci.* **2017**, *70*, 1–17.
- (23) Huang, C.; Thomas, N. L. Fabrication of porous fibers via electrospinning: strategies and applications. *Polym. Rev.* **2020**, *60*, 595–647
- (24) McCann, J. T.; Marquez, M.; Xia, Y. Highly Porous Fibers by Electrospinning into a Cryogenic Liquid. *J. Am. Chem. Soc.* **2006**, *128*, 1436–1437.
- (25) Muniz, N. O.; Vechietti, F. A.; Anesi, G. R.; Guinea, G. V.; dos Santos, L. A. L. Blend-based fibers produced via centrifugal spinning and electrospinning processes: Physical and rheological properties. *J. Mater. Res.* **2020**, *35*, 2905–2916.
- (26) Gan, Y. X.; Gan, J. B. Porous Fiber Processing and Manufacturing for Energy Storage Applications. *ChemEngineering* **2020**, *4*, 59.
- (27) Hou, T.; Li, X.; Lu, Y.; Yang, B. Highly porous fibers prepared by centrifugal spinning. *Mater. Des.* **2017**, *114*, 303–311.
- (28) Doan, H. N.; Nguyen, D. K.; Vo, P. P.; Hayashi, K.; Kinashi, K.; Sakai, W.; Tsutsumi, N.; Huynh, D. P. Facile and Scalable Fabrication of Porous Polystyrene Fibers for Oil Removal by Centrifugal Spinning. ACS Omega 2019, 4, 15992–16000.
- (29) Lu, P.; Xia, Y. Maneuvering the Internal Porosity and Surface Morphology of Electrospun Polystyrene Yarns by Controlling the Solvent and Relative Humidity. *Langmuir* **2013**, *29*, 7070–7078.
- (30) Grena, B.; Alayrac, J.-B.; Levy, E.; Stolyarov, A. M.; Joannopoulos, J. D.; Fink, Y. Thermally-drawn fibers with spatially-selective porous domains. *Nat. Commun.* **2017**, *8*, 364.
- (31) Lyngaae-Jørgensen, J.; Rasmussen, K. L.; Chtcherbakova, E. A.; Utracki, L. A. Flow induced deformation of dual-phase continuity in polymer blends and alloys. Part I. *Polym. Eng. Sci.* **1999**, 39, 1060–1071.
- (32) Li, F.; Zhao, X.; Wang, H.; Chen, Q.; Wang, S.; Chen, Z.; Zhou, X.; Fan, W.; Li, Y.; You, J. Sub-100 nm Cocontinuous Structures Fabricated in Immiscible Commodity Polymer Blend with Extremely Low Volume/Viscosity Ratio. *ACS Appl. Polym. Mater.* **2019**, *1*, 124–129.
- (33) Pötschke, P.; Paul, D. R. Formation of Co-continuous Structures in Melt-Mixed Immiscible Polymer Blends. *J. Macromol. Sci., Polym. Rev.* **2003**, *43*, 87–141.

- (34) Willemse, R. C.; Posthuma de Boer, A.; van Dam, J.; Gotsis, A. D. Co-continuous morphologies in polymer blends: a new model. *Polymer* **1998**, *39*, 5879–5887.
- (35) Jordhamo, G. M.; Manson, J. A.; Sperling, L. H. Phase continuity and inversion in polymer blends and simultaneous interpenetrating networks. *Polym. Eng. Sci.* 1986, 26, 517–524.
- (36) Willemse, R. C.; Posthuma de Boer, A.; van Dam, J.; Gotsis, A. D. Co-continuous morphologies in polymer blends: the influence of the interfacial tension. *Polymer* 1999, 40, 827–834.
- (37) Sarazin, P.; Favis, B. D. Influence of temperature-induced coalescence effects on co-continuous morphology in poly(ε -caprolactone)/polystyrene blends. *Polymer* **2005**, 46, 5966–5978.
- (38) López-Barrón, C. R.; Macosko, C. W. Rheological and morphological study of cocontinuous polymer blends during coarsening. *J. Rheol.* **2012**, *56*, 1315–1334.
- (39) Gu, L.; Nessim, E. E.; Macosko, C. W. Reactive compatibilization of poly(lactic acid)/polystyrene blends and its application to preparation of hierarchically porous poly(lactic acid). *Polymer* **2018**, *134*, 104–116.
- (40) Koning, C.; Van Duin, M.; Pagnoulle, C.; Jerome, R. Strategies for compatibilization of polymer blends. *Prog. Polym. Sci.* **1998**, 23, 707–757.
- (41) Shah, R. S.; Bryant, S.; Trifkovic, M. Microstructural Rearrangements and Their Rheological Signature in Coarsening of Cocontinuous Polymer Blends. *Macromolecules* **2020**, *53*, 10918–10926.
- (42) López-Barrón, C. R.; Macosko, C. W. Rheology of compatibilized immiscible blends with droplet-matrix and cocontinuous morphologies during coarsening. *J. Rheol.* **2014**, *58*, 1935–1953.
- (43) Veenstra, H.; Van Dam, J.; Posthuma de Boer, A. On the coarsening of co-continuous morphologies in polymer blends: effect of interfacial tension, viscosity and physical cross-links. *Polymer* **2000**, *41*, 3037–3045.
- (44) Veenstra, H.; Van Dam, J.; Posthuma de Boer, A. Formation and stability of co-continuous blends with a poly(ether-ester) block copolymer around its order—disorder temperature. *Polymer* **1999**, *40*, 1119—1130.
- (45) Warsinger, D. M.; Chakraborty, S.; Tow, E. W.; Plumlee, M. H.; Bellona, C.; Loutatidou, S.; Karimi, L.; Mikelonis, A. M.; Achilli, A.; Ghassemi, A.; Padhye, L. P.; Snyder, S. A.; Curcio, S.; Vecitis, C. D.; Arafat, H. A.; Lienhard, J. H. A review of polymeric membranes and processes for potable water reuse. *Prog. Polym. Sci.* **2018**, *81*, 209–237.
- (46) Anis, S. F.; Hashaikeh, R.; Hilal, N. Microfiltration membrane processes: A review of research trends over the past decade. *J. Water Process Eng.* **2019**, 32, 100941.
- (47) Shokoohi, S.; Arefazar, A. A review on ternary immiscible polymer blends: morphology and effective parameters. *Polym. Adv. Technol.* **2009**, *20*, 433–447.
- (48) Sarazin, P.; Favis, B. D. Morphology Control in Co-continuous Poly(l-lactide)/Polystyrene Blends: A Route towards Highly Structured and Interconnected Porosity in Poly(L-lactide) Materials. *Biomacromolecules* **2003**, *4*, 1669–1679.
- (49) Hedegaard, A. T.; Gu, L.; Macosko, C. W. Effect of extensional viscosity on cocontinuity of immiscible polymer blends. *J. Rheol.* **2015**, *59*, 1397–1417.
- (50) Kou, Y.; Cheng, X.; Macosko, C. W. Polymer/Graphene Composites via Spinodal Decomposition of Miscible Polymer Blends. *Macromolecules* **2019**, *52*, 7625–7637.
- (51) Bai, L.; Fruehwirth, J. W.; Cheng, X.; Macosko, C. W. Dynamics and rheology of nonpolar bijels. *Soft Matter* **2015**, *11*, 5282–5293.
- (52) Lopez-Barron, C. R.; Macosko, C. W. Characterizing Interface Shape Evolution in Immiscible Polymer Blends via 3D Image Analysis. *Langmuir* **2009**, 25, 9392–9404.
- (53) Wang, Z.; Liu, X.; Macosko, C. W.; Bates, F. S. Nanofibers from water-extractable melt-blown immiscible polymer blends. *Polymer* **2016**, *101*, 269–273.

- (54) Epps, H. H.; Leonas, K. K. Pore Size and Air Permeability of Four Nonwoven Fabrics. *Int. Nonwovens J.* **2000**, os-9, 1558925000OS-900215.
- (55) Zhang, S.; Tang, N.; Cao, L.; Yin, X.; Yu, J.; Ding, B. Highly Integrated Polysulfone/Polyacrylonitrile/Polyamide-6 Air Filter for Multilevel Physical Sieving Airborne Particles. ACS Appl. Mater. Interfaces 2016, 8, 29062–29072.